An investigation of α-transfer reaction ^{28}Si$\left(^{20}\text{Ne},^{16}\text{O}\right)^{32}$S

M. Aygun

Department of Physics, Bitlis Eren University, Bitlis, Turkey.

Received 20 October 2020; accepted 11 February 2021

The α-transfer reaction ^{28}Si$\left(^{20}\text{Ne},^{16}\text{O}\right)^{32}$S at 52.3 and 70 MeV is examined by using the double-folding (DF) based on the optical model. The real part is obtained for ten different density distributions of ^{20}Ne projectile. For the imaginary part, the Woods-Saxon potential is used. The obtained results are compared with the experimental data of α-transfer reaction as well as the literature results. It is seen that the results are in good agreement with the data, and are better than the literature results.

Keywords: α-transfer reaction; density distribution; optical model; double folding model.

PACS: 24.10.Ht; 25.70.Hi

DOI: https://doi.org/10.31349/RevMexFis.67.041201

1. Introduction

Different nuclear reactions such as elastic scattering, inelastic scattering, knock-out, pick-up, and stripping can occur when the nuclei interact with each other. Transfer reaction is one of them. Transfer reaction can be either a nucleon or a few-nucleon cluster form such as the α-particle. If it occurs in the form of α-particle transfer that can be assumed an elementary particle due to large binding energy [1], it is called the α-transfer reaction. The α-transfer reaction is generally observed in nuclei with α-cluster structure. It is evaluated in nuclear structure studies or α-clustering of nuclei. Also, it has an important place in the studies performed on astrophysical reactions such as the helium-burning and silicon-burning [2, 3].

The alpha transfer reaction ^{28}Si$\left(^{20}\text{Ne},^{16}\text{O}\right)^{32}$S at 52.3 and 70 MeV was measured by using ICARE target facility of the Heavy Ion Laboratory of the University of Warsaw [4, 5]. The experimental data were analyzed theoretically. However, the question of whether more compatible results with experimental data could be obtained leds us to do this study.

In the present work, we investigate the sensitivity to different density distributions of α-transfer reaction ^{28}Si$\left(^{20}\text{Ne},^{16}\text{O}\right)^{32}$S. For this, we explore the entrance channel which is considered as a dominant cause of theoretical uncertainty in the analysis of the α-transfer reactions. In this context, we use ten various density distributions of ^{20}Ne projectile. We compare the theoretical results and experimental data, and suggest the most suitable density distribution(s) for the α-transfer reaction ^{28}Si$\left(^{20}\text{Ne},^{16}\text{O}\right)^{32}$S.

Section 2 shows the calculation procedure for the α-transfer reaction. Section 3 displays the density distributions of the ^{20}Ne nucleus. Section 4 gives the results and discussion. Section 5 presents the summary and conclusions.

2. Calculation procedure

We consider the ^{28}Si$\left(^{20}\text{Ne},^{16}\text{O}\right)^{32}$S reaction where the projectile ^{20}Ne is treated as the composite system ^{20}Ne = ^{16}O + α. The α-particle is transferred to the target ^{28}Si, and thus it leads to the formation of the composite target-like fragment in the exit channel ^{32}S = ^{28}Si + α. The scheme of α-transfer reaction ^{28}Si$\left(^{20}\text{Ne},^{16}\text{O}\right)^{32}$S is shown in Fig. 1.

For the theoretical analysis of ^{28}Si$\left(^{20}\text{Ne},^{16}\text{O}\right)^{32}$S reaction, the various interactions should be considered; entrance channel $\left(^{20}\text{Ne} + ^{28}\text{Si}\right)$, exit channel $\left(^{32}\text{S} + ^{16}\text{O}\right)$, core-core $\left(^{28}\text{Si} + ^{16}\text{O}\right)$, binding potentials $\left(^{16}\text{O} + \alpha \text{ and } ^{28}\text{Si} + \alpha\right)$. The calculations related to ^{28}Si$\left(^{20}\text{Ne},^{16}\text{O}\right)^{32}$S reaction require knowledge of interaction potentials for each partitions, which these potentials are described below. The cross-sections are obtained by using the code FRESCO [6].

2.1. Entrance Channel $\left(^{20}\text{Ne} + ^{28}\text{Si}\right)$

The potentials used for the entrance channel which is a dominant cause of theoretical uncertainty in the analysis of the α-transfer reactions play a significant role. With this goal, we examine the effect of the entrance channel on the cross-section of the α-transfer reaction.

The nuclear potential of the entrance channel consists of the real and the imaginary potentials. To obtain the real potential, the double folding (DF) model is used via the DFPOT code [7] which is a very valid model in nuclear physics and many studies can be found in the literature [8–12]. The nuclear matter distributions of both projectile and target nuclei are very important in the DF calculations. Thus, the real part of nuclear potential is obtained by using ten different density distributions of the ^{20}Ne nucleus assumed as a composite system, which these density distributions are explained in below. The imaginary part is thought as Woods-Saxon (WS) potential shown by

$$W(r) = -\frac{W_0}{1+\exp\left(\frac{r-R_w}{a_w}\right)},$$
$$R_w = r_w\left(A_P^{1/3} + A_T^{1/3}\right) \quad (1)$$

where W_0 is the depth, r_w is the radius, and a_w is diffuseness parameter. Thus, the nuclear potential can be written as

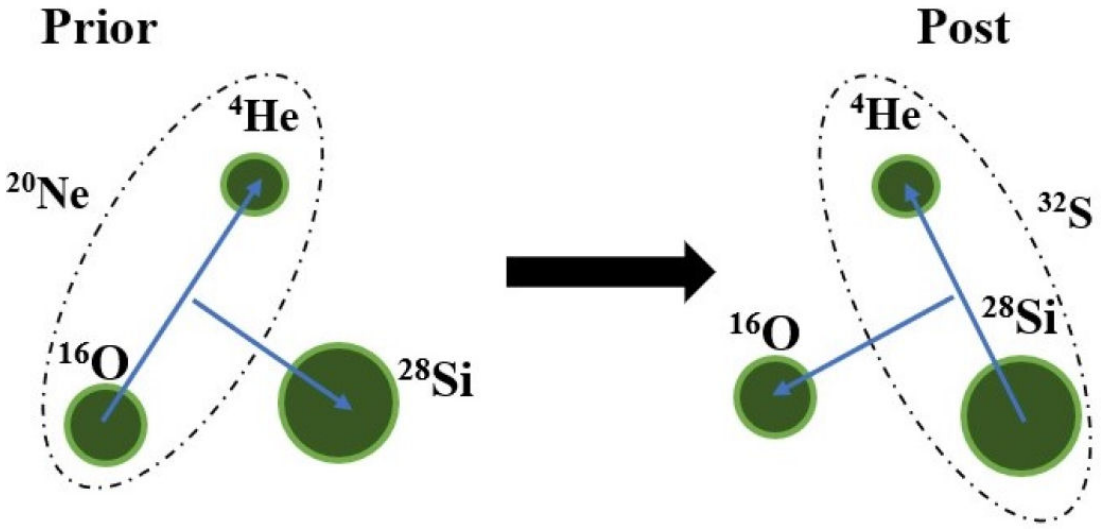

FIGURE 1. The scheme of the α-transfer reaction $^{28}\mathrm{Si}\left(^{20}\mathrm{Ne},^{16}\mathrm{O}\right)^{32}\mathrm{S}$.

TABLE I. The potential parameters used in the calculations of the nuclear potential of the entrance channel.

Channel	Density	Energy (MeV)	N_R	W_0 (MeV)	r_w (fm)	a_w (fm)
^{20}Ne + ^{28}Si	Ngo	52.3	0.968	1.00	0.90	0.50
	SP		0.990	1.10	0.90	0.50
	2pF		0.955	3.10	0.90	0.50
	G1		0.940	3.10	0.90	0.50
	G2		0.930	3.10	0.90	0.50
	J1		0.910	1.60	0.90	0.50
	J2		0.970	1.00	0.90	0.50
	M		0.920	1.30	0.90	0.50
	S		0.970	1.10	0.90	0.50
	HFB		0.953	3.50	0.90	0.50
^{20}Ne + ^{28}Si	Ngo	70	0.920	1.30	0.90	0.50
	SP		0.840	3.00	0.90	0.50
	2pF		0.680	3.00	0.90	0.50
	G1		0.890	1.00	0.90	0.50
	G2		0.850	2.00	0.90	0.50
	J1		0.950	1.00	0.90	0.50
	J2		0.863	1.00	0.90	0.50
	M		0.960	1.00	0.90	0.50
	S		0.923	1.00	0.90	0.50
	HFB		0.790	1.00	0.90	0.50

$$V_N(r) = N_R V_{NN-DF}(r) + i\frac{W_0}{1+\exp\left(\frac{r-R_w}{a_w}\right)} \qquad (2)$$

where N_R parameter is the normalization factor which is used to increase the agreement between the data and the results. The potential parameters used in the calculations with ten different density distributions are given in Table I.

2.2. Exit Channel $\left(^{32}\mathbf{S} + {}^{16}\mathbf{O}\right)$

The nuclear potential for the exit channel is assumed as the real and the imaginary potentials. In both cases the WS potential is used. Thus, the nuclear potential is formulated by

TABLE II. The potential parameters used in the calculations of the exit channel, core-core and binding potentials.

Channel	V_0 (MeV)	r_v (fm)	a_v (fm)	W_0 (MeV)	r_w (fm)	a_w (fm)
^{32}S + ^{16}O	100.0	1.22	0.50	30.0	1.25	0.40
^{16}O + ^{4}He	179.1	1.31	0.59	31.1	1.20	0.82
^{28}Si + ^{4}He	75.62	1.13	0.47	8.39	1.13	0.47
^{28}Si + ^{16}O	100.0	1.14	0.58	20.0	1.20	0.60

TABLE III. ρ_{0i}, R_i and a_i values of SP, 2pF, J1, J2, M, S densities.

Density	ρ_0	R_0	a	Ref.
SP	ρ_{0n}=0.122086	$R_n = 1.49N^{1/3} - 0.79$	$a_n = 0.47 + 0.00046N$	[15]
	ρ_{0p}=0.0873779	$R_p = 1.81Z^{1/3} - 1.12$	$a_p = 0.47 - 0.00083Z$	
2pF	ρ_{0n}=0.0736291	$R_n = 0.953N^{1/3} + 0.015Z + 0.774$	$a_n = 0.446 + 0.0072(\frac{N}{Z})$	[16]
	ρ_{0p}=0.0759015	$R_p = 1.322Z^{1/3} + 0.007N + 0.022$	$a_p = 0.449 + 0.0071(\frac{Z}{N})$	
J1	0.153545	2.805	0.571	[17]
J2	0.162812	2.740	0.569	[17]
M	0.16	$1.15A^{1/3}$	0.50	[18]
S	$\frac{0.212}{1+2.66A^{-2/3}}$	$1.04A^{1/3}$	0.54	[19]

$$V_N(r) = \frac{V_0}{1+\exp\left(\frac{r-R_v}{a_v}\right)} + i\frac{W_0}{1+\exp\left(\frac{r-R_w}{a_w}\right)} \qquad (3)$$

The parameters of the potentials used in the calculations are taken from Ref. [5], and are listed in Table II.

2.3. Core-Core (^{28}Si + ^{16}O)

The core-core potential describes the interaction between core and core nuclei. This potential is evaluated as the sum of the real and the imaginary potentials in the WS shape. As a result of this, the nuclear potential is the same with Eq. (3). The parameters of the potentials taken from Ref. [5] are given in Table II.

2.4. Binding potentials

The binding potentials for ^{28}Si$(^{20}$Ne,^{16}O$)^{32}$S reaction are considered as binding potential: entrance potential and binding potential: exit channel. The binding potential for the entrance potential is ^{16}O + α, and the binding potential for exit channel is ^{28}Si + α. The real and imaginary potentials for binding potentials are used in the WS form as similar to Eq. (3). In this context, the parameters used in the calculations are gotten from Ref. [5], and are shown in Table II.

3. Density distributions of ^{20}Ne nucleus

3.1. Ngô (Ngo) density

The Ngo density can be formulated as [13, 14]

$$\rho_{n(p)}(r) = \frac{\frac{3}{4\pi}\frac{N(Z)}{A}\frac{1}{r_{0n(0p)}^3}}{1+\exp\left(\frac{r-C}{0.55}\right)}, \quad C = R\left(1-\frac{1}{R^2}\right), \quad (4)$$

where

$$R = \frac{Nr_{0n}A^{1/3} + Zr_{0p}A^{1/3}}{A},$$
$$r_{0n} = 1.1375 + 1.875\times10^{-4}A,$$
$$r_{0p} = 1.128\,\text{fm}. \qquad (5)$$

3.2. São Paulo (SP), Two parameter Fermi (2pF), Jager 1 (J1), Jager 2 (J2), Moszkowski (M), Schechter (S) densities

The SP [15], 2pF [16], J1 [17], J2 [17], M [18], S [19] densities can be taken as the two parameter Fermi

$$\rho_i(r) = \frac{\rho_{0i}}{1+\exp\left(\frac{r-R_i}{a_i}\right)}, \quad (i=n,p) \qquad (6)$$

where ρ_{0i}, R_i and a_i parameters are listed in Table III.

3.3. Gupta 1 (G1) density

The G1 density is shown by [20, 21]

$$\rho_i(r) = \frac{\rho_{0i}}{1+\exp\left(\frac{r-R_{0i}}{a_i}\right)},$$

$$\rho_{0i} = \frac{3A_i}{4\pi R_{0i}^3}\left(1+\frac{\pi^2 a_i^2}{R_{0i}^2}\right)^{-1}, \quad (7)$$

where

$$R_{0i} = 0.90106 + 0.10957A_i - 0.0013A_i^2 + 7.71458\times10^{-6}A_i^3 - 1.62164\times10^{-8}A_i^4, \quad (8)$$

$$a_i = 0.34175 + 0.01234A_i - 2.1864\times10^{-4}A_i^2 + 1.46388\times10^{-6}A_i^3 - 3.24263\times10^{-9}A_i^4. \quad (9)$$

3.4. Gupta 2 (G2) density

The G2 density [22] is presented with different values of R_{0i} and a_i given by

$$R_{0i} = 0.9543 + 0.0994A_i - 9.8851\times10^{-4}A_i^2 + 4.8399\times10^{-6}A_i^3 - 8.4366\times10^{-9}A_i^4, \quad (10)$$

$$a_i = 0.3719 + 0.0086A_i - 1.1898\times10^{-4}A_i^2 + 6.1678\times10^{-7}A_i^3 - 1.0721\times10^{-9}A_i^4. \quad (11)$$

3.5. Hartree-Fock-Bogolubov (HFB) density

The HFB density is based on the BSk2 Skyrme force calculations [23]. In our study, the HFB density is gotten from RIPL-3 [23].

4. Results and discussion

The α-transfer reaction ^{28}Si$(^{20}$Ne,^{16}O$)^{32}$S at 52.3 and 70 MeV was examined for ten different density distributions of

TABLE IV. The rms radii for the Ngo, SP, 2pF, G1, G2, J1, J2, M, S and HFB density distributions.

Density distribution	rms radii (fm)
Ngo	2.955
SP	2.665
2pF	2.847
G1	2.789
G2	2.734
J1	3.037
J2	2.996
M	3.049
S	2.968
HFB	2.842

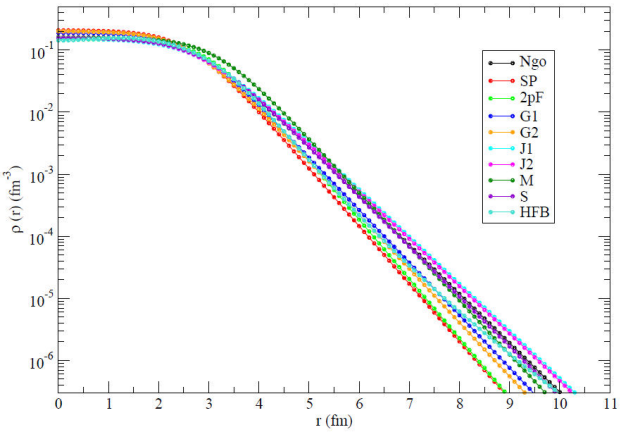

FIGURE 2. The changes with the distance (r) of Ngo, SP, 2pF, G1, G2, J1, J2, M, S, and HFB density distributions in logarithmic scale.

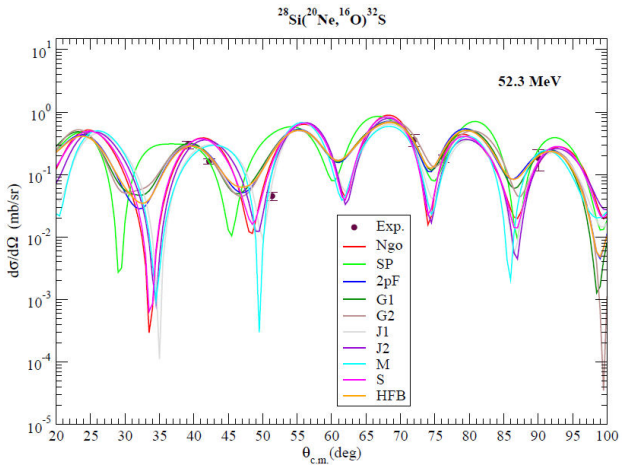

FIGURE 3. The cross-sections calculated for the α-transfer reaction ^{28}Si$(^{20}$Ne,^{16}O$)^{32}$S by using Ngo, SP, 2pF, G1, G2, J1, J2, M, S, and HFB densities in comparison with the experimental data at 52.3 MeV. The experimental data are taken from Ref. [5].

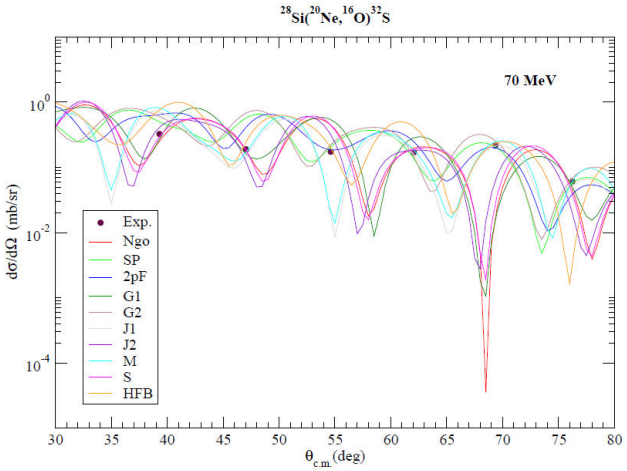

FIGURE 4. Same as Fig. 3, but for 70 MeV. The experimental data are taken from Ref. [5].

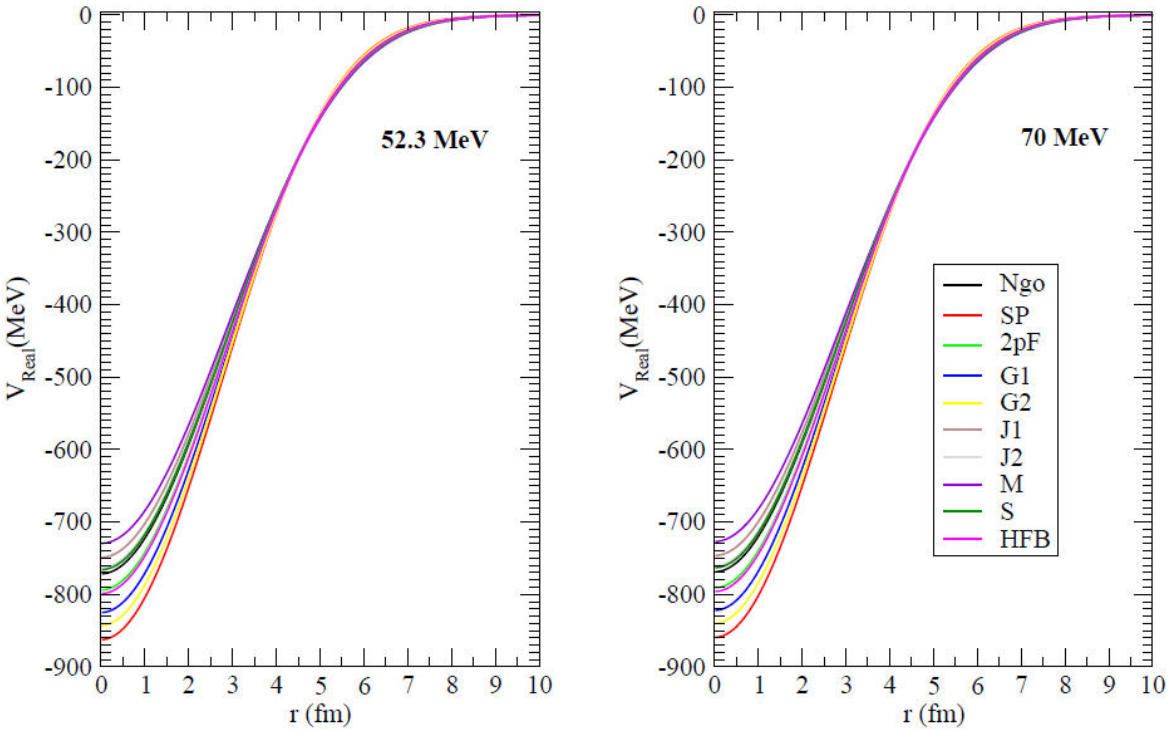

FIGURE 5. The changes with the distance (r) of the real potential depths calculated for Ngo, SP, 2pF, G1, G2, J1, J2, M, S, and HFB densities at 52.3 and 70 MeV.

^{20}Ne projectile which consist of Ngo, SP, 2pF, G1, G2, J1, J2, M, S, and HFB densities. The changes with the distance (r) of the densities were presented in Fig. 2. The highest density in the center part was seen for the SP density while the lowest density was found for the HFB density. Moreover, the root mean square (rms) values of the density distributions were listed in Table IV.

We first calculated the cross-section of the alpha transfer reaction ^{28}Si$(^{20}$Ne,^{16}O$)^{32}$S at 52.3 MeV by using ten different densities of ^{20}Ne nucleus for the entrance channel. We compared the theoretical results with the experimental data in Fig. 3. We observed that the result of G1 density is slightly better than the result of 2pF density although the results of G1 and 2pF densities appear to behave close to each other. At the same time, the results of G1, G2 and HFB densities were found to be very close to each other up to 70 degrees, whereas it was seen that there was little difference at further angles. However, it can be said that very good results for G1, G2 and HFB density distributions are yielded although the results of G1 and G2 densities were slightly better than the HFB density.

Then, we calculated the cross-section of the α-transfer reaction ^{28}Si$(^{20}$Ne,^{16}O$)^{32}$S at 70 MeV. We showed the results as compared with the experimental data in Fig. 4. We observed that the results of SP, G2, M and S density distributions are very good in defining the experimental data. As a result of this, we propose more than one alternative density distribution for the analysis of the alpha transfer reaction ^{28}Si$(^{20}$Ne,^{16}O$)^{32}$S.

In our study, we observed that cross-section results for all the density distributions are very sensitive to the N_R constant used in the calculations of the DF model. When we examined the density distributions in this sense, we found the lowest value for J1 density and the highest value for SP density at 52.3 MeV, and the lowest value for 2pF density and the highest value for M density at 70 MeV. This shows that the real potential of the entrance channel is very effective in the analysis of the α-transfer reaction.

We also demonstrated the change with the distance (r) of the real parts of the nuclear potential for each density distribution in Fig. 5. In this context, the shallowest potential was obtained for the M density while the deepest potential was found for the SP density.

Finally, we compared the literature results [5] with the best theoretical results for 52.3 and 70 MeV in Fig. 6. We observed that G1 and G2 results are better than the result of Ref. [5] at 52.3 MeV. Similarly, we noticed that the results of SP, G2, M and S densities are better than the result of Ref. [5] at 70 MeV. As a result of this, it can be said that the density distributions examined in this study have provided a significant correction on the cross-section of α-transfer reaction ^{28}Si$(^{20}$Ne,^{16}O$)^{32}$S, and can be used as alternative density distributions in future studies related to α-transfer reactions.

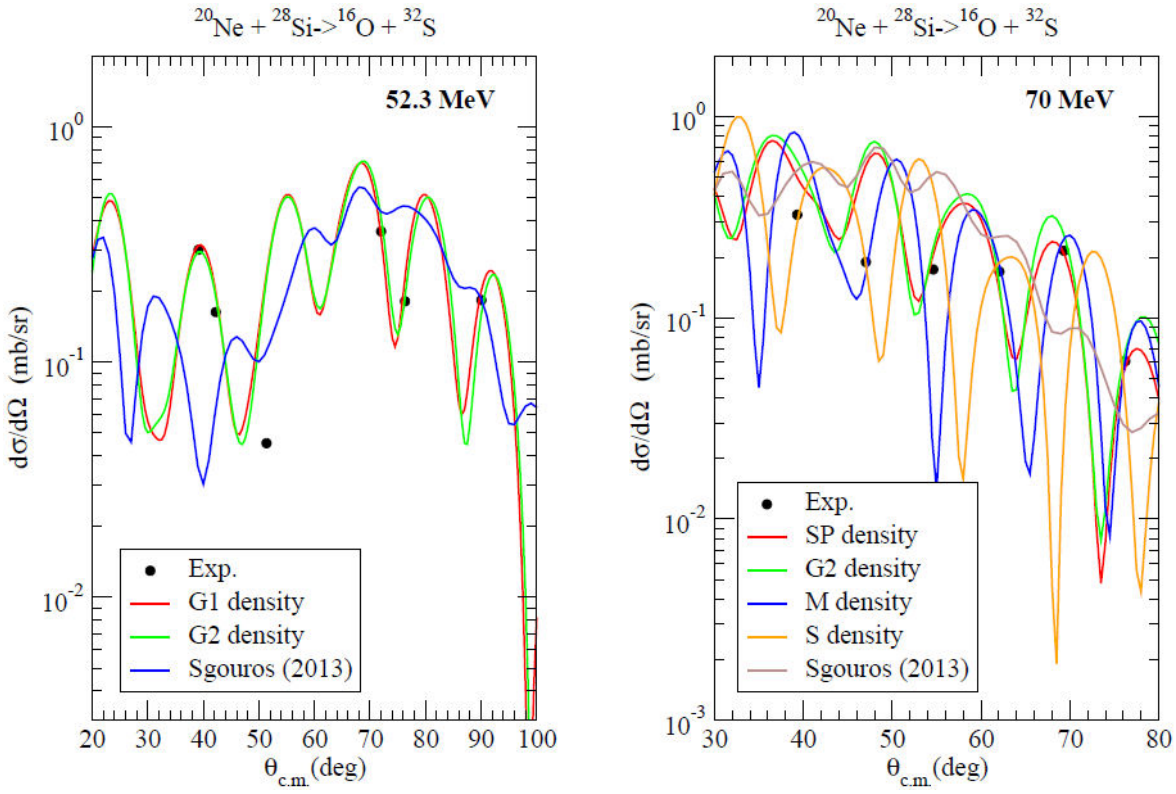

FIGURE 6. Comparison of the literature results with the best theoretical results at 52.3 and 70 MeV.

5. Summary and conclusions

In this work, the α-transfer reaction ^{28}Si$(^{20}$Ne,^{16}O$)^{32}$S at 52.3 and 70 MeV was investigated for the entrance potential that is dominant in transfer reactions. The cross-sections were calculated for Ngo, SP, 2pF, G1, G2, J1, J2, M, S, and HFB density distributions of ^{20}Ne projectile. It was observed that the G1 and G2 densities at 52.3 MeV, and the SP, G2, M and S densities at 70 MeV provided satisfactory results to the α-transfer experimental data. Also, it was observed they were better than both other density distributions and literature results. As a result of this, we can say that these densities will be alternative in the theoretical analysis of the α-transfer reactions. Additionally, we deduced that the entrance channel is very effective in the theoretical analysis of the α-transfer reaction ^{28}Si$(^{20}$Ne,^{16}O$)^{32}$S. We think it would be useful to apply this approach to other transfer reactions.

1. T. Madhusoodhanan *et al.*, Study of α-transfer reaction ^{28}Si(^{7}Li,t)^{32}S, *J. Phys. G: Nucl. Part. Phys.* **25** (1999) 1897, https://doi.org/10.1088/0954-3899/25/9/309.
2. D. J. Pisano and P. D. Parker, Alpha-transfer reactions in light nuclei. II. (^{3}He,^{7}Be) pickup reaction, *Phys. Rev. C* **14** (1976) 475, https://doi.org/10.1103/PhysRevC.14.475.
3. A. Kr. Mondal *et al.*, Study of α-transfer process in the ^{12}C(^{20}Ne,^{16}O)^{16}O reaction at E_{lab} = 150 MeV, *Proceedings of the DAE Symp. on Nucl. Phys.* **63** (2018).
4. O. Sgouros *et al.*, Backward angle structure in the ^{20}Ne+^{28}Si quasielastic scattering, *Int. J. Mod. Phys. E* **22** (2013) 1350073, https://doi.org/10.1142/S0218301313500730.
5. O. Sgouros, *Transfer reactions for the system ^{20}Ne+^{28}Si at near barrier energies*, Master Thesis, University of Ioannina 2013.
6. I. J. Thompson, Coupled reaction channels calculations in nuclear-physics, *Comp. Phys. Rep.* **7** (1988) 167, https://doi.org/10.1016/0167-7977(88)90005-6.
7. J. Cook, DFPOT-A program for the calculation of double folded potentials, *Comput. Phys. Commun.* **25** (1982) 125, https://doi.org/10.1016/0010-4655(82)90029-7.
8. T. Ulucay and M. Aygun, A comprehensive description of elastic scattering angular distributions for eight different density distribution of ^{32}S nucleus, *Rev. Mex. Fis.* **66** (2020) 336, https://doi.org/10.31349/RevMexFis.66.336.
9. M. Aygun and Z. Aygun, A comprehensive analysis of ^{9}Li+^{70}Zn fusion cross section by using proximity potentials,

temperature dependent density distributions and nuclear potentials, *Rev. Mex. Fis*. **65** (2019) 573, https://doi.org/10.31349/RevMexFis.65.573.

10. M. Aygun and Z. Aygun, Microscopic analysis of elastic scattering cross sections for different densities of ^{8}Li nucleus on light, medium and heavy mass targets, *Rev. Mex. Fis*. **65** (2019) 404, https://doi.org/10.31349/RevMexFis.65.404.
11. M. Aygun, A comprehensive study on the internal structure and thedensity distribution of ^{12}Be, *Rev. Mex. Fis*. **62** (2016) 336.
12. M. Aygun, O. Kocadag and Y. Sahin, Phenomenological and microscopic model analysis of elastic scattering reactions of ^{18}O by ^{24}Mg, ^{28}Si, ^{58}Ni, ^{64}Zn, ^{90}Zr, ^{120}Sn, and ^{208}Pb target nuclei, *Rev. Mex. Fis*. **61** (2015) 414.
13. C. Ngô *et al.*, Properties of heavy ion interaction potentials calculated in the energy density formalism, *Nucl. Phys. A* **252** (1975) 237, https://doi.org/10.1016/0375-9474(75)90614-4.
14. H. Ngô and C. Ngô, Calculation of the real part of the interaction potential between two heavy ions in the sudden approximation, *Nucl. Phys. A* **348** (1980) 140, https://doi.org/10.1016/0375-9474(80)90550-3.
15. L. C. Chamon *et al.*, Toward a global description of the nucleus-nucleus interaction, *Phys. Rev. C* **66** (2002) 014610, https://doi.org/10.1103/PhysRevC.66.014610.
16. W. M. Seif and H. Mansour, Systematics of nucleon density distributions and neutron skin of nuclei, *Int. J. Mod. Phys. E* **24** (2015) 1550083, https://doi.org/10.1142/S0218301315500834.
17. C. W. De Jager, H. De Vries and C. De Vries, Nuclear charge- and magnetization-density-distribution parameters from elastic electron scattering, *At. Data Nucl. Data Tables* **14** (1974) 479, https://doi.org/10.1016/S0092-640X(74)80002-1.
18. S. A. Moszkowski, Energy dependence of the ion-ion potential with a simplified energy density method, *Nucl. Phys. A* **309** (1978) 273, https://doi.org/10.1016/0375-9474(78)90548-1.
19. H. Schechter and L. F. Canto, Proximity formulae for folding potentials, *Nucl. Phys. A* **315** (1979) 470, https://doi.org/10.1016/0375-9474(79)90623-7.
20. R. K. Gupta, D. Singh and W. Greiner, Semiclassical and microscopic calculations of the spin-orbit density part of the Skyrme nucleus-nucleus interaction potential with temperature effects included, *Phys. Rev. C* **75** (2007) 024603, https://doi.org/10.1103/PhysRevC.75.024603.
21. O. N. Ghodsi and F. Torabi, Comparative study of fusion barriers using Skyrme interactions and the energy density functional, *Phys. Rev. C* **92** (2015) 064612, https://doi.org/10.1103/PhysRevC.92.064612.
22. R. K. Gupta, D. Singh, R. Kumar and W. Greiner, Universal functions of nuclear proximity potential for Skyrme nucleus-nucleus interaction in a semiclassical approach, *J. Phys. G: Nucl. Part. Phys*. **36** (2009) 075104, https://doi.org/10.1088/0954-3899/36/7/075104.
23. http://www-nds.iaea.org/ripl-3.html.